Multiple Flow Equilibria in the Atmosphere and Blocking[1]

JULE G. CHARNEY[2]
Massachusetts Institute of Technology, Cambridge 02139

JOHN G. DEVORE[3]
University of California, Los Angeles 90024

(Manuscript received 22 September 1978, in final form 28 February 1979)

ABSTRACT

A barotropic channel model is used to study the planetary-scale motions of an atmosphere whose zonal flow is externally driven. Perturbations are induced by topography and by a barotropic analogue of thermal driving. The use of highly truncated spectral expansions shows that there may exist a multiplicity of equilibrium states for a given driving, of which two or more may be stable. In the case of topographical forcing, two stable equilibrium states of very different character may be produced by the same forcing: one is a "low-index" flow with a strong wave component and a relatively weaker zonal component which is locked close to linear resonance; the other is a "high-index" flow with a weak wave component and a relatively stronger zonal component which is much farther from linear resonance. It is suggested that the phenomenon of blocking is a metastable equilibrium state of the low-index, near-resonant character. The existence of the two types of equilibria has been confirmed by numerical integration of a grid-point model with many more degrees of freedom than the spectral model.

It has also been found spectrally and for a grid-point model that oscillations may occur when one of the equilibrium states is stable for the lowest order spectral components but unstable for the next higher order components. The oscillation apparently is due to a barotropic instability of the topographic wave of the kind discussed by Lorenz and Gill.

Thermal forcing also produces multiple, stable equilibria in a spectral model but confirmation with a grid-point model has so far not been obtained.

1. Introduction

It is common to regard the flow of the atmosphere as a quasi-stationary circulation of large scale on which are superimposed transient wave and vortex disturbances of smaller scale originating as instabilities of the mean flow and interacting with it. The mean or equilibrium state is often thought of as a Hadley circulation perturbed by fixed topographic and thermal asymmetries of the lower boundary. But this description, while it has permitted a qualitative explanation of many of the observed features of the global circulation, has left others entirely unexplained. In particular it has not accounted for the persistence of large amplitude flow anomalies such as blocking. Nor has it explained the existence, well-known to synoptic meteorologists, of the persistent or recurrent regional weather patterns or types exemplified by the *grosswetterlage* of Baur (1951).[4] Do such patterns originate from the interaction of smaller scale instabilities with a single large-scale equilibrium flow?

We wish to answer this question in the negative by presenting evidence that suggests that there is a *multiplicity* of stationary or oscillatory states, each presumably with its own class of smaller scale instabilities and each presumably capable of undergoing transition with the aid of these instabilities from one to another. We do so by analyzing a simple model of a barotropic atmosphere in which an externally forced zonal flow interacts nonlinearly with topography and with externally forced wave perturbations. We show that in each case there is a multiplicity of equilibrium states, two or more of which may be stable, and that when one of these becomes unstable, self-excited oscillations may also occur. Among the equilibrium flows are some in which the flow is a large-amplitude perturbation of

[1] The research reported in this work was sponsored by the National Science Foundation under Grants ATM 78-22424 and ATM 77-24843, and by the Office of Naval Research under Contract N00014-78-C-0103. It was presented to the meeting of the European Geophysical Society in Strasbourg 29 August 1978.

[2] The research was done while on a leave at the Department of Atmospheric Sciences, University of California, Los Angeles.

[3] On leave from General Electric TEMPO, Santa Barbara, CA 93102.

[4] See also Namias (1943, 1953) and Elliot (1951).

0022-4928/79/071205-12$07.00

the zonal westerlies arising from the nonlinear locking of the zonal flow close to resonance. These bear a marked resemblance to blocking flows.

Our work arose from a seminar course conducted by the senior author on large-scale long-period variability in the atmosphere. In an effort to explain the generation of transient planetary Rossby waves, he was led to extend a result of Hirota's (1971) that the interaction of a fluctuating zonal flow with topography will produce a forced propagating oscillation which will appear as a free-propagating Rossby wave. He suggested that the large-scale wave zonal flow interaction might be unstable and itself produce a self-excited oscillation, and he proposed that the seminar should study the properties of a highly truncated spectral model of topographically perturbed channel flow in a barotropic atmosphere. This was done, and two types of self-excited oscillations were found—the first, however, only for inviscid flows. This one arises from a purely topographically induced instability of the equilibrium flow, which cannot exist without the interaction of the perturbation with the topography. The second is apparently a barotropic vacillation arising from a barotropic shear instability of the topographic wave of the kind discussed by Lorenz (1972) and Gill (1974). When driving forces and friction were included, the oscillations due to the first instability damped to zero. Inquiring into the causes of the damping, the authors discovered the existence of two additional equilibrium states. These were stable, and when the system was perturbed from the unstable state, it fell into the phase-space attractor basin of one or another of the stable equilibrium states and approached that state on a direct or spiral path. The finding of multiple equilibria in a non-axisymmetric, forced system appears to be new and suggests a fresh approach to the study of atmospheric phenomena on long space and time scales.

2. The model

The actual atmosphere is of course baroclinic, but all of the phenomena to be considered have their counterparts in the simpler barotropic atmosphere. Thus questions involving topographic forcing, resonance and nonlinear interaction via the advective terms in the equations of motion may be studied barotropically. For example, the prototypical quasi-equilibrium phenomenon of blocking has been found by Egger (1978) in numerical simulations of the flow of a barotropic atmosphere over topography. It is true that such phenomena as baroclinic instability and vertical propagation of energy are not present in a barotropic model, but the former occurs on scales that are smaller than those we wish to study, and the latter does not occur when the waves are trapped vertically as by easterlies or strong westerlies (Charney and Drazin, 1961; Charney, 1969). Baroclinic instabilities may be important but in the present context only as additional forcing of the planetary-scale motions.

We shall therefore take as our model a homogeneous β-plane atmosphere with a free surface of height $H + \eta$ and mean height H confined between zonal walls a distance πL apart. The lower boundary elevation will be denoted by $h(x,y)$, where x is the eastward directed coordinate and y the northward directed coordinate. Since the motions will be of large scale, they will be quasi-geostrophic and therefore governed by conservation of potential vorticity (Charney, 1974)

$$\left(\frac{\partial}{\partial t} + u\frac{\partial}{\partial x} + v\frac{\partial}{\partial y}\right)\frac{\zeta + f_0 + \beta y}{1 + (\eta - h)/H} \approx \frac{\partial}{\partial t}\times\left(\nabla^2\psi - \frac{\psi}{\lambda^2}\right) + J\left(\psi, \nabla^2\psi - \frac{\psi}{\lambda^2} + f_0\frac{h}{H} + \beta y\right) = -f_0\frac{D_E}{2H}\nabla^2(\psi - \psi^*), \quad (1)$$

where u and v are the x and y velocity components, ∇ is the horizontal gradient operator, J is the Jacobian operator, $f_0 = 2\Omega\sin\phi_0$, $\beta = 2\Omega\cos\phi_0/a$, Ω is the angular speed of the earth's rotation, a the radius of the earth, ϕ_0 a central latitude, $\psi = g\eta/f_0$, $u = -\partial\psi/\partial y$, $v = \partial\psi/\partial x$, $\zeta = \partial v/\partial x - \partial u/\partial y = \nabla^2\psi$, and $\lambda^2 = gH/f_0^2$. In deriving (1), it is assumed that $|h| \ll H$ and that $\pi L \ll 2a$, although the latter requirement may be relaxed without violating conservation of potential vorticity but at the expense of some flow distortion. The motion is retarded by a frictionally induced vorticity sink given by $-f_0 w_E/H$, where w_E is the Ekman pumping, $(D_E/2)\nabla^2\psi$, with D_E the Ekman depth $(2\nu_E/f_0)^{1/2}$ and ν_E the bulk eddy viscosity in the frictional boundary layer. It is accelerated by the momentum source (U,V) giving rise to the vorticity source $\partial V/\partial x - \partial U/\partial y \equiv (f_0 D_E/(2H))\nabla^2\psi^*$. In a baroclinic atmospheric (U,V) would be the thermal wind driven by the radiation field.

To simplify the problem further, we expand ψ, ψ^* and h in orthonormal eigenfunctions of the Laplace operator, which, for the channel flow under consideration, are simply trigonometric functions. Thus

$$\left.\begin{aligned}(\psi,\psi^*) &= L^2 f_0 \sum_{i=1}^{\infty}(\psi_i,\psi_i^*)F_i,\\ h &= H\sum_{i=1}^{\infty} h_i F_i,\end{aligned}\right\} \quad (2)$$

where

$$L^2\nabla^2 F_i = -a_i^2 F_i, \quad (3)$$

and

$$\frac{\partial F_i}{\partial x} = 0 \quad \text{at} \quad y = 0, \pi L \quad (4)$$

to satisfy the condition of no normal flow at the boundaries.

This procedure closely parallels that of Lorenz (1963) who derived similar spectral equations for a two-layer channel flow model in his study of the mechanics of vacillation. Our equations differ from his only in applying to a single layer and in including the effects of topography and variations of the Coriolis parameter. Like Lorenz, we omit reference to all but a finite set of eigenfunctions, choosing the six functions

$$\left.\begin{aligned} F_1 &= F_A = \sqrt{2}\cos\frac{y}{L}, & F_2 &= F_K = 2\cos\frac{nx}{L}\sin\frac{y}{L} \\ F_3 &= F_L = 2\sin\frac{nx}{L}\sin\frac{y}{L}, & F_4 &= F_C = \sqrt{2}\cos\frac{2y}{L} \\ F_5 &= F_M = 2\cos\frac{nx}{L}\sin\frac{2y}{L}, & F_6 &= F_N = 2\sin\frac{nx}{L}\sin\frac{2y}{L} \end{aligned}\right\}, \tag{5}$$

and setting

$$\psi = \sum_{i=1}^{6}\psi_i F_i = \psi_A F_A + \psi_K F_K + \psi_L F_L + \psi_C F_C + \psi_M F_M + \psi_N F_N, \tag{6}$$

with similar expressions for ψ^* and h. The first orthogonal function, F_A, permits a zonal flow component which varies from zero at the boundaries to a maximum at the center of the channel; the fourth (F_C) permits a zonal flow component with both a maximum and a minimum in the interior. The y-amplitudes of the corresponding pairs of wave functions (F_K,F_L) and (F_M,F_N) have, respectively, one and two maxima in the interior. Both pairs are needed if wave-wave interactions are to occur. Thus if we wish to simulate the effects of thermal asymmetries of the lower boundary, we must introduce wave driving as well as zonal flow driving, and in this case it is the wave-wave interaction that permits multiple stationary equilibria.

If F_j and F_k are two arbitrary eigenfunctions, then owing to their orthonormal property

$$L^2 J(F_j,F_k) = \sum_{i=1}^{\infty} c_{ijk}F_i, \tag{7}$$

where

$$c_{ijk} = L^2\overline{F_i J(F_j,F_k)}, \tag{8}$$

with the bar denoting a horizontal average. It follows by definition that $c_{ijk} = -c_{ikj}$, and from the boundary conditions that $c_{ijk} = c_{jki} = c_{kij}$.

If we nondimensionalize t by f_0^{-1}, x and y by L, ψ and ψ^* by $L^2 f_0$, and h by H, (1) becomes

$$\frac{\partial}{\partial t}\left(\nabla^2\psi - \frac{\psi}{\lambda^2}\right) + J(\psi, \nabla^2\psi + h) + \bar{\beta}\frac{\partial\psi}{\partial x} + k\nabla^2(\psi - \psi^*) = 0, \tag{9}$$

where λ^2 is now $gH/(f_0^2L^2)$, $\bar{\beta} = (L/a)\cot\phi_0 = (L/a)$ at 45°, and $k = D_E/(2H) = (E/2)^{1/2}$, where E is the Ekman number $\nu_E/(f_0H^2)$. Setting

$$\frac{\partial F_i}{\partial x} = \sum_{j=1}^{\infty} b_{ij}F_j, \quad b_{ij} = F_i\frac{\overline{\partial F_i}}{\partial x},$$

we obtain

$$\dot{\psi}_i = (a_i^2 + \lambda^{-2})^{-1}\{\sum_{k>j}^{\infty} c_{ijk} \times [(a_j^2 - a_k^2)\psi_j\psi_k - h_j\psi_k + h_k\psi_j] + \bar{\beta}\sum_{j=1}^{\infty} b_{ji}\psi_j - ka_i^2(\psi_i - \psi_i^*)\}. \tag{10}$$

For simplicity and to ensure that we are dealing with large topographic scales, we consider only the first topographic wave mode K

$$h \text{ (dimensional)} = h_0\cos\frac{nx}{L}\sin\frac{y}{L}$$

or

$$h \text{ (nondimensional)} = \frac{h_0}{2H}F_k.$$

Then we obtain

$$\dot{\psi}_A = -k_{01}(\psi_A - \psi_A^*) + h_{01}\psi_L, \tag{11}$$

$$\dot{\psi}_k = -(\alpha_{n1}\psi_A - \beta_{n1})\psi_L - \delta_{n1}\psi_C\psi_N - k_{n1}(\psi_K - \psi_K^*), \tag{12}$$

$$\dot{\psi}_L = (\alpha_{n1}\psi_A - \beta_{n1})\psi_K + \delta_{n1}\psi_C\psi_M - k_{n1}(\psi_L - \psi_L^*) - h_{n1}\psi_A, \tag{13}$$

$$\dot{\psi}_c = \epsilon_n(\psi_K\psi_N - \psi_L\psi_M) - k_{02}(\psi_C - \psi_C^*) + h_{02}\psi_N, \tag{14}$$

$$\dot{\psi}_M = -(\alpha_{n2}\psi_A - \beta_{n2})\psi_N - \delta_{n2}\psi_C\psi_L - k_{n2}(\psi_M - \psi_M^*), \tag{15}$$

$$\dot{\psi}_N = (\alpha_{n2}\psi_A - \beta_{n2})\psi_M + \delta_{n2}\psi_C\psi_K - k_{n2}(\psi_N - \psi_N^*) + h_{n2}\psi_C, \tag{16}$$

where

$$\left.\begin{aligned}
\frac{\gamma_{n1}}{5} &= \frac{\gamma_{n2}}{4} = \frac{\gamma_{n3}}{8} = \frac{8\sqrt{2}}{15\pi}\, n \\
\alpha_{nm} &= \frac{n^2 + m^2 - 1}{n^2 + m^2 + \lambda^{-2}}\,\gamma_{nm} \\
\delta_{nm} &= \frac{n^2 - m^2 + 1}{n^2 + m^2 + \lambda^{-2}}\,\gamma_{n3} \\
\epsilon_n &= \frac{3\gamma_{n3}}{4 + \lambda^{-2}} \\
k_{nm} &= \frac{n^2 + m^2}{n^2 + m^2 + \lambda^{-2}}\,k \\
\beta_{nm} &= \frac{n}{n^2 + m^2 + \lambda^{-2}}\,\frac{L}{a}\cot\phi_0 \\
h_{01} &= \frac{\gamma_{n1}}{1 + \lambda^{-2}}\,\frac{h_0}{2H} \\
h_{02} &= \frac{\gamma_{n3}}{4 + \lambda^{-2}}\,\frac{h_0}{2H} \\
h_{n1} &= \frac{\gamma_{n1}}{n^2 + 1 + \lambda^{-2}}\,\frac{h_0}{2H} \\
h_{n2} &= \frac{\gamma_{n3}}{n^2 + 4 + \lambda^{-2}}\,\frac{h_0}{2H}
\end{aligned}\right\} \quad (17)$$

Assuming the topographical effect of the stretching and compression of the vortex tubes of the earth's rotation to be confined to the troposphere, we set $H = 10^4$ m as an approximation to the height of the tropopause. If it were desired to simulate as accurately as possible the phase velocity of the dominant free or forced Rossby wave modes in a baroclinic atmosphere with the observed vertical density structure, the acceleration of gravity g should be chosen so as to give the correct "equivalent height" for the actual atmosphere. In the case of traveling free Rossby waves the results of Diky and Golitsyn (1968) suggest $4\Omega^2a^2/gH = 8.8$, or $g = 3.6$ m sec^{-2} for $H = 10^4$ m. However, since verisimilitude is not our primary aim, it will be more convenient to set $g = \infty$, $\lambda^{-2} = 0$, i.e., to replace the upper free surface by a rigid horizontal boundary.

3. Multiple equilibrium states for topographically driven disturbances of a zonal flow

a. Topographic instability

Let us consider first the conservative case by setting ψ^* and k equal to zero. Then if the second y-mode quantities ψ_C, ψ_M and ψ_N are zero initially, they will remain zero and the system will be governed by

$$\dot{\psi}_A = h_{01}\psi_L, \quad (18)$$

$$\dot{\psi}_K = -(\alpha_{n1}\psi_A - \beta_{n1})\psi_L, \quad (19)$$

$$\dot{\psi}_L = (\alpha_{n1}\psi_A - \beta_{n1})\psi_K - h_{n1}\psi_A. \quad (20)$$

At equilibrium ψ_A is arbitrary, $\psi_L = 0$ and $\psi_K = h_{n1}\psi_A/b_{n1}$, where

$$b_{n1} = \alpha_{n1}\psi_A - \beta_{n1} = \frac{40\sqrt{2}}{15\pi}\,\frac{n^3}{n^2 + 1}\,\psi_A - \frac{L}{a}\,\frac{n}{n^2 + 1}\cot\phi_0. \quad (21)$$

Small perturbations from this state are governed by the linearized equations

$$\dot{\psi}'_A = h_{01}\psi'_L, \quad (22)$$

$$\dot{\psi}'_K = -\bar{b}_{n1}\psi'_L, \quad (23)$$

$$\dot{\psi}'_L = \bar{b}_{n1}\psi'_K + (\alpha_{n1}\bar{\psi}_K - h_{n1})\psi'_A = \bar{b}_{n1}\psi'_K + \frac{\beta_{n1}h_{n1}}{\bar{b}_{n1}}\,\psi'_A, \quad (24)$$

where the overbars refer to equilibrium values and the primes to perturbations. Differentiating (24) and substituting from (22) and (23) we find

$$\ddot{\psi}'_L + \left(\bar{b}_{n1}^2 - \frac{\beta_{n1}h_{01}h_{n1}}{\bar{b}_{n1}}\right)\psi'_L = 0, \quad (25)$$

from which it follows that the solution $e^{\sigma t}$ grows exponentially with time if

$$\sigma^2 = \frac{\beta_{n1}h_{01}h_{n1}}{\bar{b}_{n1}} - \bar{b}_{n1}^2 > 0, \quad (26)$$

i.e., if $\bar{b}_{n1} > 0$ and $\beta_{n1}h_{01}h_{n1} > \bar{b}_{n1}^3$. Indeed, the growth rate approaches infinity as $\bar{b}_{n1}$ approaches zero through positive values and $\bar{\psi}_K = h_{n1}\bar{\psi}_A/\bar{b}_{n1}$ becomes resonantly amplified.

Dr. Julia Paegle, a member of the seminar to which we have referred, has pointed out that the system (18)–(20) possesses two constants of the motion, the energy,

$$\tfrac{1}{2}[\psi_A^2 + (n^2 + 1)(\psi_K^2 + \psi_L^2)] = E,$$

and the quantity

$$\tfrac{1}{2}[b_{n1}^2 + 2\alpha_{n1}h_{01}\psi_K] = G,$$

which may be derived from (9) as a combination of energy and potential enstrophy in spectral terms. With the aid of these first integrals she was able to integrate the system in terms of elliptic functions and thereby to show that the system is periodic.

b. Multiple equilibria in the truncated spectral model

We next introduce zonal driving and dissipation in the first y mode by fixing ψ_A^* and setting the other

spectral components of ψ^* in (11)–(16) equal to zero. The quantity ψ_A^* is the driving Rossby number $U_0/(\sqrt{2}Lf_0)$, where U_0 is the dimensional amplitude of the forcing zonal wind profile.

Again we note that if the second y-mode components are zero initially they will remain zero. The system will then be governed by

$$\dot{\psi}_A = -k(\psi_A - \psi_A^*) + h_{01}\psi_L, \tag{27}$$

$$\dot{\psi}_K = -k\psi_K - b_{n1}\psi_L, \tag{28}$$

$$\dot{\psi}_L = -k\psi_L + b_{n1}\psi_K - h_{n1}\psi_A. \tag{29}$$

At equilibrium these equations yield

$$\frac{\psi_L}{h_{n1}} = \frac{k}{h_{01}h_{n1}}(\psi_A - \psi_A^*), \tag{30}$$

$$\frac{\psi_L}{h_{n1}} = -\frac{k}{b_{n1}^2 + k^2}\psi_A, \tag{31}$$

$$\frac{\psi_K}{h_{n1}} = \frac{b_{n1}}{b_{n1}^2 + k^2}\psi_A, \tag{32}$$

from which ψ_A, ψ_K and ψ_L can be found by equating (30) and (31), solving the resulting cubic equation,

$$(\psi_A - \psi_A^*)[(\alpha_{n1}\psi_A - \beta_{n1})^2 + k^2] + h_{01}h_{n1}\psi_A = 0, \tag{33}$$

for ψ_A, and substituting in (31) and (32). The curves in the ψ_A, ψ_L/h_{n1} plane representing (30) and (31) are shown in Fig. 1 for $k = 10^{-2}$, $L/a = \frac{1}{4}$, $n = 2$, $\psi_A^* = 0.05, 0.1, 0.2$, and $h_0/H = 0.05, 0.1, 0.2$, corresponding to an exponential decay time of about 11 days and to a wavelength and channel width πL of 5000 km centered at 45°. The intersection of a straight line given by (30) with the curve defined by (31) gives ψ_A and ψ_L/h_{n1} at equilibrium. It will be seen that for an appreciable range of parameter values there are three separate equilibrium values of ψ_A, two of which are close to and on either side of the resonant value $\psi_A = \beta_{n1}/\alpha_{n1}$. The third is close to ψ_A^*.

The stability of an equilibrium solution is determined from the characteristic values of the sixth order coefficient matrix of the linear perturbation equations resulting from (11)–(16), i.e., from

$$\begin{vmatrix} -(\sigma+k) & 0 & h_{01} & 0 & 0 & 0 \\ -\alpha_{n1}\bar{\psi}_L & -(\sigma+k) & -\bar{b}_{n1} & 0 & 0 & 0 \\ \alpha_{n1}\bar{\psi}_K - h_{n1} & \bar{b}_{n1} & -(\sigma+k) & 0 & 0 & 0 \\ 0 & 0 & 0 & -(\sigma+k) & -\epsilon_n\bar{\psi}_L & \epsilon_n\bar{\psi}_K + h_{02} \\ 0 & 0 & 0 & -\delta_{n2}\bar{\psi}_L & -(\sigma+k) & -\bar{b}_{n2} \\ 0 & 0 & 0 & \delta_{n2}\bar{\psi}_K - h_{n2} & \bar{b}_{n2} & -(\sigma+k) \end{vmatrix} = 0, \tag{34}$$

where

$$\bar{b}_{n2} = \alpha_{n2}\bar{\psi}_A - \beta_{n2} = \frac{32\sqrt{2}n}{15\pi}\frac{n^2+3}{n^2+4}\bar{\psi}_A - \frac{n}{n^2+4}\frac{L}{a}\cot\phi_0.$$

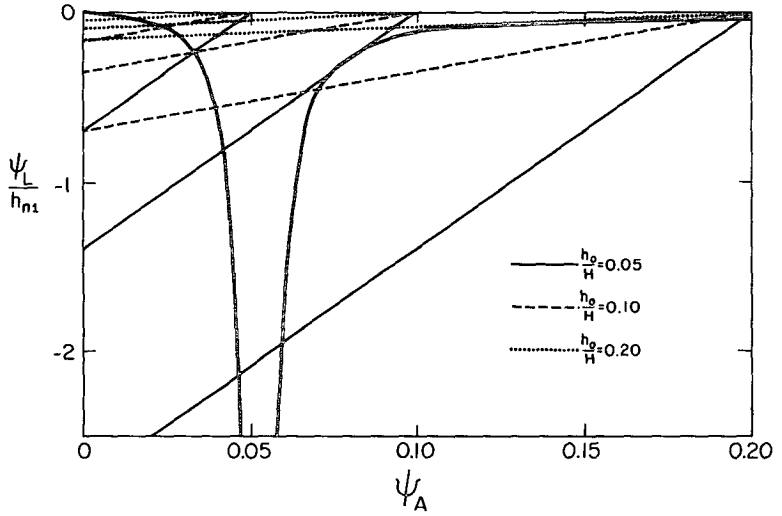

FIG. 1. Graphical solution of the equations governing the first mode equilibria of a topographically driven flow. The heavy curve corresponds to Eq. (31) and the lighter lines to Eq. (30). The intersections of the straight lines with the ψ_A axis determines ψ_A^*.

TABLE 1. First mode equilibria of a topographically driven flow for $k = 10^{-2}$, $L/a = \frac{1}{4}$, $n = 2$ and $h_0/H = 0.2$.

				max σ_{real}	
ψ_A^*	ψ_A	ψ_K	ψ_L	Mode 1	Mode 2
0.05	0.0153	−0.0102	−0.00145	−0.0089	−0.0090
	—	—	—	—	—
	—	—	—	—	—
0.1	0.0224	−0.0184	−0.00323	−0.0082	−0.0076
	—	—	—	—	—
	—	—	—	—	—
0.2	0.154	0.0377	−0.00194	−0.0046	−0.0084
	0.121	0.0436	−0.00328	0.011	−0.0067
	0.0294	−0.0309	−0.00710	−0.0074	−0.0005
0.25	0.227	0.0324	−0.00970	−0.0086	−0.0095
	0.0958	0.0540	−0.00642	0.0845	−0.0024
	0.0315	−0.0360	−0.00910	−0.0072	0.0060
0.3	0.283	0.0306	−0.00069	−0.0093	−0.0097
	0.0876	0.0604	−0.00885	0.108	0.0012
	0.0331	−0.0405	−0.0111	−0.0070	0.0231
0.4	0.389	0.0289	−0.00045	−0.0097	−0.0099
	0.0794	0.0701	−0.0134	0.132	0.0086
	0.0354	−0.0485	−0.0152	−0.0068	0.0473
0.5	0.492	0.0280	−0.00033	−0.0098	−0.0099
	0.0750	0.0778	−0.0177	0.147	0.0168
	0.0371	−0.0554	−0.0193	−0.0066	0.0624

The characteristic equation is of the sixth degree but factors into two cubics whose roots correspond to first and second y-mode perturbations, respectively. The equilibrium values of ψ_A, ψ_K and ψ_L, together with the maximum real parts of the σ triads for each of the two perturbation modes, are shown in Table 1 for $k = 10^{-2}$, $L/a = \frac{1}{4}$, $n = 2$, and $h_0/H = 0.2$. It is seen that when there is only one equilibrium, it is always stable, and that when there are three, the one with the intermediate value of ψ_A is unstable; the other two remain stable for first mode perturbations, but the one with the smaller value of ψ_A (on the low side of resonance) becomes unstable for second mode perturbations when the zonal driving ψ_A^* is sufficiently large. Thus there is a range of values of ψ_A^* for which two stable equilibria exist.

The intermediate equilibrium occurs for $\bar{b}_{n1} > 0$ and its instability corresponds to that already found for the inviscid case. This instability seems to be new. Apparently, it is not a simple barotropic instability of the zonal flow, since the zonal flow profile is a half sine wave for which the gradient of the absolute vertical vorticity component $\beta - \partial^2\bar{u}/\partial y^2$ does not vanish. Nor is it a wave instability of the kind studied by Lorenz (1972), Gill (1974), and Coaker (1977) for plane waves on an infinite β-plane, or by Hoskins (1973) for Rossby-Haurwitz waves on a sphere, since these instabilities require a second wave mode. It is solely due to the interaction of the topographic wave with the zonal mean flow.

If there were only the single unstable equilibrium state, one would expect a small perturbation to result in some type of oscillation, but integration of the time-dependent first mode equations for the nonconservative case does not show this. What does occur can be described in the first mode phase space whose coordinates are ψ_A, ψ_K and ψ_L, and in the extended phase space whose coordinates are ψ_A, ψ_K, ψ_L, ψ_C, ψ_M, and ψ_N. A point in the first mode phase space close to the unstable fixed point finds itself in the attractor basin of one or the other of the two stable fixed points and winds down into one of them. Fig. 2 shows an example of such behavior for an experiment started near an unstable middle-index state that finds a stable low-index state. However, when one of the stable fixed points becomes unstable for mixed mode perturbations, its representative point in the extended phase space need not find itself in the attractor basin of the other stable fixed point, and the system may oscillate. Unlike the first mode instability, the mixed mode instability does not vanish when the topographic amplitude in the perturbation equation goes to zero. Thus in the limiting case $k = 0$ we find $\bar{\psi}_L = 0$, and the cubic in σ derived from (34) for second mode perturbations becomes

$$\sigma[\sigma^2 - \epsilon_n\delta_{n2}(\bar{\psi}_K)^2 + (\bar{b}_{n2})^2] = 0,$$

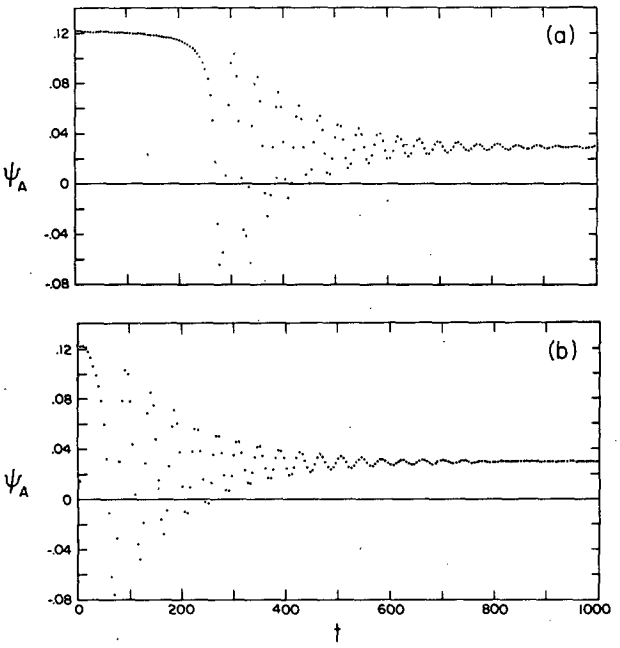

FIG. 2. Transition from an unstable, first mode, middle-index state to a stable, first mode, low-index state for $k = 10^{-2}$, $L/a = \frac{1}{4}$, $n = 2$, $h_0/H = 0.2$ and $\psi_A^* = 0.2$. ψ_A^* is plotted versus time for the spectral model (a) and the grid point model (b).

which has a positive real root if

$$\epsilon_n \delta_{n2} (\bar{\psi}_K)^2 > (\bar{b}_{n2})^2.$$

This instability does appear to be analogous to the wave instability of Lorenz and Gill. As Gill has shown, it can be a Rayleigh-like or a resonant triad instability according as the parameter $\bar{\psi}_K/\beta_{n1}$ (in our notation) is order unity or small. In the present case this parameter is order unity and the instability is of the Rayleigh type.

An example of the oscillatory behavior mentioned above was found for the mixed mode spectral system for $k = 10^{-2}$, $L/a = \frac{1}{4}$, $n = 2$, $h_0/H = 0.2$, and $\psi_A^* = 0.25$. Table 1 shows an equilibrium state just below resonance that is unstable to second mode perturbations. A time dependent numerical calculation started at this state with small second mode perturbations went into a stable oscillation. Figure 3 shows the development of the oscillation in ψ_A and ψ_C. The period of the oscillation of ψ_A with the spectral model is about 100 time units or 11 days.

Mixed mode equilibrium states may also occur for the system (11)–(16). If we equate the time derivative terms to zero, the wave components ψ_K, ψ_L, ψ_M, and ψ_N may be eliminated to give the following two equations in ψ_A and $X = \delta_{n1}\delta_{n2}\psi_C^2$:

$$\left.\begin{aligned} &X^2 + [h_{n1}h_{n2}p_1 + 2(k^2 - b_{n1}b_{n2})]X + (k^2 + b_{n1}^2)(k^2 + b_{n2}^2) - h_{n1}^2 p_1 p_2 = 0, \\ &X^2 + \left[- \frac{h_{01}h_{n1}p_3}{\delta_{n2}(\psi_A - \psi_A^*)} + 2(k^2 - b_{n1}b_{n2}) \right] X + (k^2 + b_{n1}^2)(k^2 + b_{n2}^2) + \frac{h_{01}h_{n1}\psi_A(k^2 + b_{n2}^2)}{(\psi_A - \psi_A^*)} = 0 \end{aligned}\right\}, \quad (35)$$

where

$$p_1 = \frac{\epsilon_n \psi_A + \rho_{0n}(b_{n1} + b_{n2})}{\rho_{n0}\epsilon_n(\psi_A - \psi_A^*) + (b_{n1} + b_{n2})},$$

$$p_2 = \delta_{n2}\psi_A(b_{n1} + b_{n2}) - \rho_{nn}(k^2 + b_{n1}^2),$$

$$p_3 = \delta_{n2}\psi_A - \rho_{nn}(b_{n1} + b_{n2}),$$

$$\rho_{ij} = \frac{h_{i2}}{h_{j1}} = \frac{8}{5}\frac{j^2 + 1}{i^2 + 4}.$$

These equations may be solved numerically for ψ_A and X and the remaining ψ components determined from

$$\psi_M = \psi_C[h_{n1}\delta_{n2}\psi_A(kk_n - b_{n1}b_n) + h_{n2}b_n(k^2 + b_{n1}^2)]/(k_n^2 + b_n^2),$$

$$\psi_N = \psi_C[h_{n1}\delta_{n2}\psi_A(kb_n + b_{n1}k_n) - h_{n2}k_n(k^2 + b_{n1}^2)]/(k_n^2 + b_n^2),$$

$$\psi_K = -[\delta_{n1}\psi_C(k\psi_N + b_{n1}\psi_M) - h_{n1}b_{n1}\psi_A]/(k^2 + b_{n1}^2),$$

$$\psi_L = -[\delta_{n1}\psi_C(b_{n1}\psi_N - k\psi_M) + h_{n1}k\psi_A]/(k^2 + b_{n1}^2),$$

where

$$b_n = b_{n2}(k^2 + b_{n1}^2) - b_{n1}X,$$

$$k_n = k(k^2 + b_{n1}^2) + kX.$$

We note that the mixed mode solutions occur in pairs in which ψ_A, ψ_K and ψ_L are the same but ψ_C, ψ_M and ψ_N are opposite in sign. It is found that there may exist one or more pairs of mixed mode equilibrium states for a range of ψ_A near linear resonance. Their stabilities are determined from the characteristic values of the linear perturbation equation coefficient matrix, which in this case factors into a first- and fifth-degree equation. An example with two pairs of mixed mode states occurs for $\psi_A^* = 0.17$, $k = 10^{-2}$, $L/a = \frac{1}{4}$, $n = 2$, $h_0/H = 0.1$. The states are $(\psi_A, \psi_K, \psi_L, \psi_C, \psi_M, \psi_N) = (0.0496, 0.0150, -0.0100, \pm 0.0225, \pm 0.0168, \mp 0.0029)$ and $(0.0659, 0.0173, -0.0087, \pm 0.0320, \pm 0.0105, \pm 0.0006)$. All of these are found to be unstable. For the same values of k, L/a and n, but for $\psi_A^* = 0.1$ and $h_0/H = 0.05$ we find 1) a stable first mode state far above resonance $(\psi_A, \psi_K, \psi_L) = (0.0852, 0.0157, -0.00246)$; 2) an unstable first mode state just above resonance; 3) a first mode state just below resonance $(\psi_A, \psi_K, \psi_L) = (0.0415, -0.0198, -0.00975)$, which is stable to first mode perturbations and unstable to second mode perturbations; and 4) a pair of stable mixed mode states $(\psi_A, \psi_K, \psi_L, \psi_C, \psi_M, \psi_N) = (0.0357, -0.0098, -0.0108, \pm 0.00679, \pm 0.00063, \mp 0.0115)$.

c. *Multiple equilibria in a grid-point model*

Numerical integrations of (9) were carried out on a 16×16 grid for the same geometry, driving and dissipation as in the spectral model, and with initial conditions taken as equilibrium solutions of the truncated spectral model. The Arakawa (1966)

energy and enstrophy conserving finite difference scheme was used. In the case $\psi_A^* = 0.2, h_0/H = 0.2$, and for $L/a = \frac{1}{4}, n = 2, k = 10^{-2}$, Table 1 gives the stable equilibrium values, $(\psi_A, \psi_K, \psi_L) = (0.154, 0.0377, -0.0019)$ and $(0.0294, -0.0309, -0.0071)$ for the spectral model. In each case a damped oscillation occurred, and after several dissipation times or about a month, the solutions had effectively converged to stationary states. Spectral decomposition into (ψ_A, ψ_K, ψ_L) then gives $(0.153, 0.0399, -0.0026)$ and $(0.0290, -0.0312, -0.0088)$ for the two equilibrium states of the grid point model (taken as 750 time units). These compare well with the corresponding values for the spectral model. The streamfunction fields of the equilibrium states for the spectral and grid-point models are shown in Fig. 4. The agreement between the two calculations verifies that the given driving and topography do indeed allow two stable, stationary flows.

The grid-point model with many degrees of freedom also confirmed the results of the truncated spectral model for the oscillating flow mentioned above, i.e., for $k = 10^{-2}$, $L/a = \frac{1}{4}$, $n = 2$, $h_0/H = 0.2$, and $\psi_A^* = 0.25$. Both the oscillating behavior for an initial condition given by the spectrally unstable first mode equilibrium state just below resonance, $(\psi_A, \psi_K, \psi_L) = (0.0315, -0.0360, -0.0091)$, and the stationary behavior given by the spectrally stable, high-index, first mode equilibrium state above resonance, $(\psi_A, \psi_K, \psi_L) = (0.227, 0.0324, -0.0001)$, were verified by the grid model calculations. It may be seen from Fig. 3, which compares the first and second mode zonal streamfunction amplitudes ψ_A and ψ_C for the spectral and grid models, that their behavior is qualitatively similar. For the high-index equilibrium the grid calculation gives $(\psi_A, \psi_K, \psi_L) = (0.227, 0.0339, -0.0012)$ after 500 time units or nearly two months, which compares well with the spectral equilibrium values. Examination of the evolution of the stream fields in both the spectral and grid models shows that the low-index oscillation is a barotropic vacillation in which the tilt of the wave trough and ridge lines fluctuates and with the aid of topography produces a fluctuating exchange of wave and zonal momentum.

The behavior of the truncated spectral model was not always confirmed by the grid model. In the previously mentioned case, $k = 10^{-2}$, $L/a = \frac{1}{4}$, $n = 2$, $h_0/H = 0.05$, and $\psi_A^* = 0.1$, the spectral model possessed a pair of stable mixed mode states, a stable high-index first mode state, and an oscillatory low-index first mode state. Experiments with the grid-point model initialized to the various spectral states all resulted in oscillations in the vicinity of a low-index state.

The two equilibrium states that were found with the spectral model and confirmed with the grid-point model are analogues of the observed quasi-stationary flow configurations produced by topographic and thermal forcing, *viz.*, the normal configuration characterized by relatively weak perturbations of the zonal flow and the blocking configuration characterized by a strong meridional flow. The Pacific and Atlantic blocking ridges are located

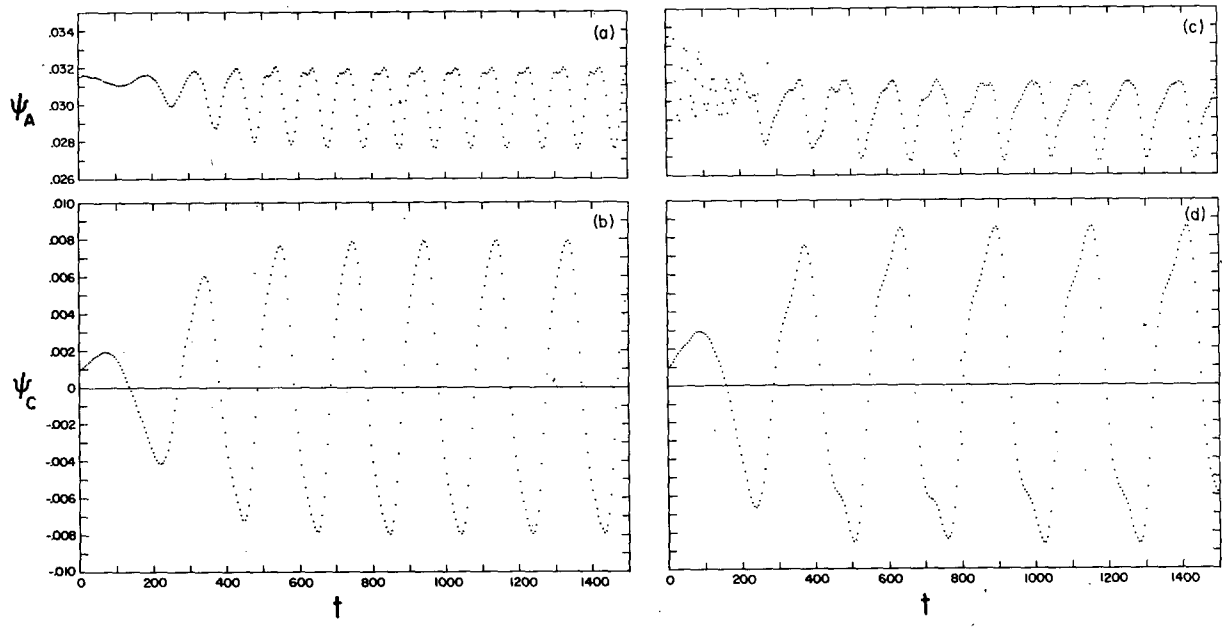

FIG. 3. Oscillation of a topographically forced flow for $k = 10^{-2}$, $L/a = \frac{1}{4}$, $n = 2$, $h_0/H = 0.2$ and $\psi_A^* = 0.25$. (a) and (b) are the first and second mode zonal streamfunction amplitudes as a function of time for the truncated spectral model; (c) and (d) are for the grid-point model.

west of the principle topographic barriers of North America and Europe. Fig. 4 shows that this is also true of the ridges in the models. The amplitudes of the Pacific and Atlantic blocking patterns are comparable in magnitude although the European barriers, consisting of the Spanish Plateau, the Pyrenees, the Alps, the Apennines and the Scandinavian mountain ranges, are on the average lower than the North American Cordillera. This may be because the amplitudes are only weakly dependent or not at all dependent on the topographic amplitudes. Thus we find from the data in Fig. 1 that the wave amplitudes are in the ratios 1:0.94:0.84 for $h_0/H = 0.05$, 0.10, 0.20, respectively, i.e., a 400% increase in mountain height causes a 16 percent *decrease* in amplitude. In reality, of course, the flows are baroclinic, and a blocking pattern once established can maintain itself only by converting potential energy. The mountain barrier effect may be merely the triggering and phase-fixing mechanism.

4. Multiple equilibrium states for thermally driven flows

In a baroclinic atmosphere, thermal asymmetries of the lower boundary drive a zonally asymmetric thermal wind. The analogous driving in a barotropic atmosphere is the direct forcing of the flow wave field. Again, if the forcing occurs in the first mode only, a self-contained flow involving only this mode will occur. We postulate the same geometry and dissipation as in the topographic case, but we force the wave component ψ_K^* as well as the zonal component ψ_A^*. The remaining components of ψ^* are set equal to zero. The equations governing the motion are then (11)–(16) with $h = \psi_C^* = \psi_M^* = \psi_N^* = 0$. When only first mode spectral components are allowed, a single equilibrium state exists which is given by $\psi_A = \psi_A^*$, $\psi_K = k^2(k^2 + b_{n1}^2)^{-1}\psi_K^*$ and $\psi_L = b_{n1}k(k^2 + b_{n1}^2)^{-1}\psi_K^*$. When second mode components are allowed, the six equilibrium equations derived from (11)–(16) yield the additional solutions

$$
\begin{aligned}
\psi_A &= \psi_A^*, \\
\psi_M &= \pm[\mu_1\mu_2(\psi_K^*)^2]^{-1}\{b_{n1}b_{n2} - k^2 \\
&\qquad \pm k[\delta_{n2}\epsilon_n(\psi_K^*)^2 - (b_{n1} + b_{n2})^2]^{1/2}\}^{1/2}, \\
\psi_C &= -\epsilon_n\psi_K^*(b_{n1} + b_{n2})^{-1}\psi_M, \\
\psi_N &= \frac{1}{k}\left[-b_{n1} + \frac{(b_{n1} + b_{n2})(k^2 + b_{n1}^2) - k^2\mu_2(\psi_K^*)^2}{k^2 + b_{n1}^2 + \mu_1\mu_2(\psi_K^*)^2(\psi_M)^2}\right]\psi_M, \qquad (36) \\
\psi_K &= \psi_K^*(k^2 + b_{n1}^2)^{-1}[k^2 + \mu_1\psi_M(b_{n1}\psi_M + k\psi_N)], \\
\psi_L &= \psi_K^*(k^2 + b_{n1}^2)^{-1}[b_{n1}k - \mu_1\psi_M(k\psi_M - b_{n1}\psi_N)],
\end{aligned}
$$

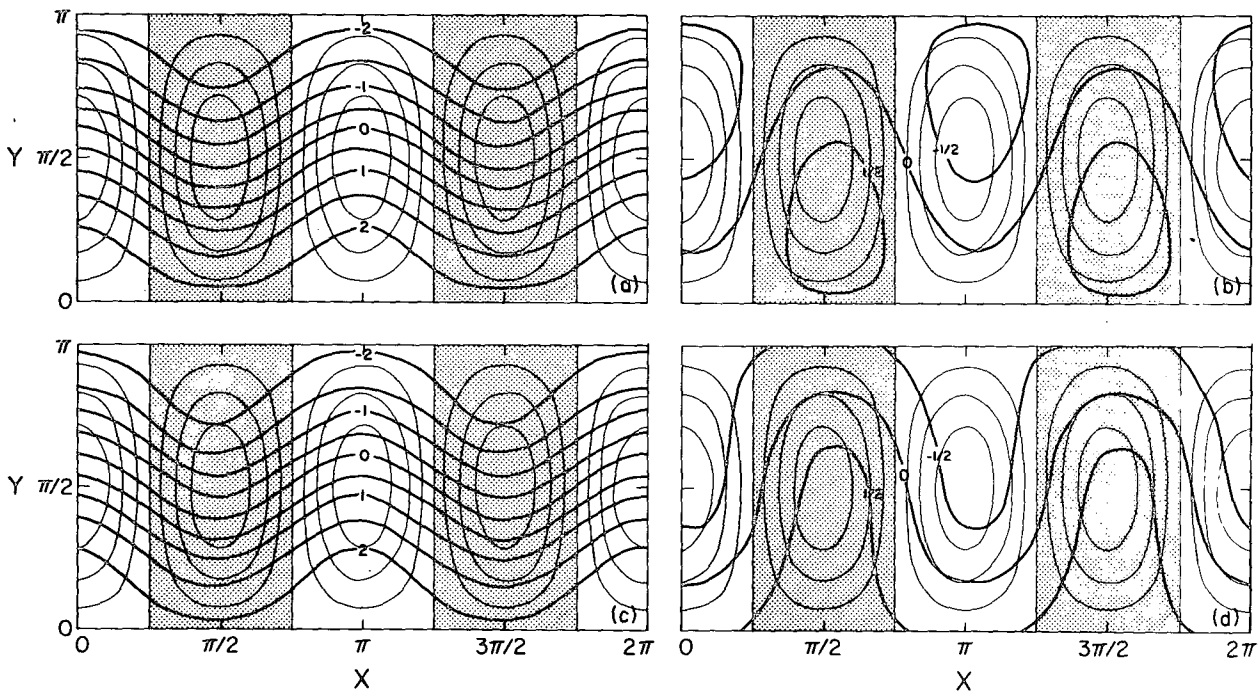

FIG. 4. Streamfunction fields of the stable first mode equilibria of a topographically forced flow for $k = 10^{-2}$, $L/a = \frac{1}{4}$, $n = 2$, $h_0/H = 0.2$ and $\psi_A^* = 0.2$: for the spectral model above resonance (a) and slightly below resonance (b); and for the grid-point model above resonance (c) and slightly below resonance (d). The nondimensional topographic heights are shown with light lines; the contour spacing is 0.05 units, with negative regions shaded.

where

$$b_{nm} = \alpha_{nm}\psi_A^* - \beta_{nm},$$

$$\mu_m = \frac{\delta_{nm}\epsilon_n}{(b_{n1} + b_{n2})}.$$

Set $Y = \delta_{n2}\epsilon_n(\psi_K^*)^2$. Then if

$$k^2[Y - (b_{n1} + b_{n2})^2] > (b_{n1}b_{n2} - k^2)^2,$$

or

$$k^2Y > (k^2 + b_{n1}^2)(k^2 + b_{n2}^2), \quad (37)$$

there will be two additional pairs of solutions. If

$$0 < k^2[Y - (b_{n1} + b_{n2})^2] < (b_{n1}b_{n2} - k^2)^2$$

or

$$k^2(b_{n1} + b_{n2})^2 < k^2Y < (k^2 + b_{n1}^2)(k^2 + b_{n2}^2), \quad (38)$$

there will be zero or four additional pairs of solutions according as $b_{n1}b_{n2} - k^2 \lesseqgtr 0$. If

$$Y < (b_{n1} + b_{n2})^2 \quad (39)$$

there will be none. The individual pairs are of the form $(\psi_A, \psi_K, \psi_L, \pm\psi_C, \pm\psi_M, \pm\psi_N)$, as in the mixed mode topographic equilibria, and their stabilities are independent of their parities.

The stability equation for the first mode equilibrium state may be derived from (34) by setting $h_0 = 0$. As before, it reduces to a product of the cubics,

$$(\sigma + k)[(\sigma + k)^2 + b_{n1}^2] = 0 \quad (40)$$

and

$$(\sigma + k)[(\sigma + k)^2 + b_{n2}^2 - k^2(b_{n1}^2 + k^2)^{-1}Y] = 0, \quad (41)$$

corresponding to perturbations of the first and second modes, respectively. We note that the roots of (40) are negative or complex with negative real parts and that the condition for positive σ in (41) is

$$k^2Y > (k^2 + b_{n1}^2)(k^2 + b_{n2}^2),$$

i.e., the same as (37). Thus if the first mode equilibrium is unstable, there will be two pairs of mixed mode equilibrium solutions. If the first mode equilibrium is stable, there may be zero or four such pairs depending on the conditions (38) and (39).

Table 2 gives the spectral components of the various equilibrium states of a thermally-driven flow for $k = 10^{-2}$, $L/a = \frac{1}{4}$, $n = 2$, $\psi_K^* = 0.05$, and $\psi_A^* = 0.02$, 0.04, 0.06 and 0.08. The table also lists the maximum real parts of the growth rate σ for small perturbations. It will be seen that several stable equilibrium states may exist, some of which are characterized by weak zonal flows and large wave amplitudes. The streamfunctions of the stable first and mixed mode equilibria for $\psi_A^* = 0.06$ and $\psi_K^* = 0.05$ were used as initial conditions for grid-point calculations. At the termination of the calculations both solutions appeared to be slowly converging to a state which resembles the stable first mode spectral equilibrium. Streamfunction fields for the first and mixed mode states of the spectral model and the final state of a grid point model calculation after 750 time units, or nearly three months, are shown in Fig. 5.

5. Conclusions

The existence of highly persistent or recurrent anomalies of the atmospheric circulation, of which blocking is an example, has long been known. It is a challenge to dynamic meteorologists to find an explanation for these phenomena. In this article we suggest that they are associated with the occurrence of multiple stationary or oscillatory equilibrium states for given external forcing. Utilizing a highly truncated spectral model of a barotropic atmosphere, in which both zonal and wave components of the flow can be forced externally, we have shown that more than one stable equilibrium state can exist when a zonal flow is forced over topography or when both zonal and wave components are externally forced, as by thermal asymmetries of the lower boundary. In the case of topographically forced disturbances of a zonal flow, the presence of multiple stable equilibria has been verified by numerical

TABLE 2. Equilibria of a thermally driven flow for $k = 10^{-2}$, $L/a = \frac{1}{4}$, $n = 2$, $h_0/H = 0$ and $\psi_K^* = 0.05$.

ψ_A^*	ψ_A	ψ_K	ψ_L	ψ_C	ψ_M	ψ_N	max σ_{real}
0.02	0.02	0.00128	−0.00791	—	—	—	−0.0100
0.04	0.04	0.00785	−0.0182	—	—	—	0.0128
	0.04	0.00681	−0.00648	0.0154	0.00197	0.00596	−0.00701
	0.04	0.00681	−0.00648	−0.0154	−0.00197	−0.00596	−0.00701
0.06	0.06	0.0150	0.0229	—	—	—	−0.0100
	0.06	0.0332	−0.00569	−0.0222	0.00825	−0.00374	−0.00697
	0.06	0.0332	−0.00569	0.0222	−0.00825	0.00374	−0.00697
	0.06	0.0262	0.0212	−0.0128	0.00476	0.00215	0.00514
	0.06	0.0262	0.0212	0.0128	−0.00476	−0.00215	0.00514
0.08	0.08	0.00168	0.00901	—	—	—	−0.0100

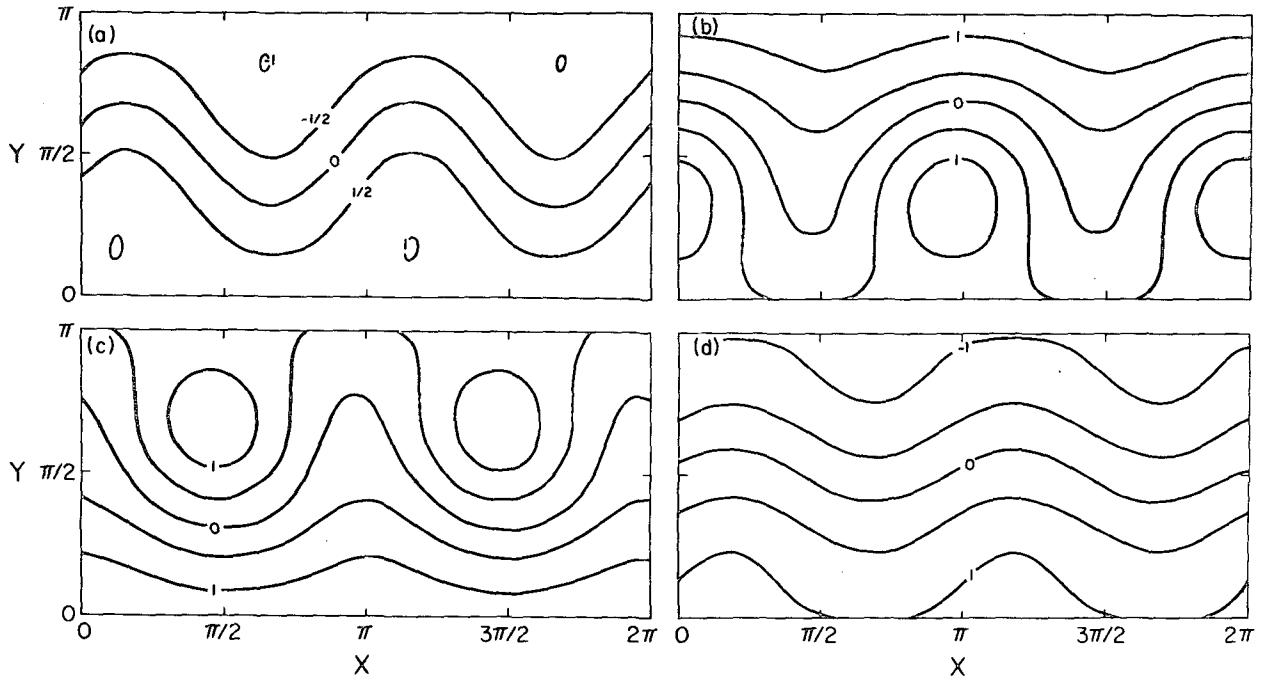

FIG. 5. Streamfunction fields of the stable equilibria of a thermally driven flow for $k = 10^{-2}$, $L/a = \frac{1}{4}$, $n = 2$, $h_0/H = 0$, $\psi_R^* = 0.05$, and $\psi_A^* = 0.06$: for the spectral model in a first-mode state (a) and in mixed-mode states (b,c); and for the grid-point model after 750 time units (d).

integration of a grid model with many more degrees of freedom than the spectral model. In the case of the barotropic equivalent of thermal forcing, multiple stable equilibria have not been found with the grid model.

Some of the equilibrium flows are locked close to linear resonance and have large-amplitude wave components. This is the analogue of the blocking configuration. What is not accounted for in any linear resonance theory is the fact that the interactions with topography or with asymmetric thermal driving are highly nonlinear and, indeed, it is the nonlinearity that produces the locking in to a near-resonant state. Such a state is found in the topographic case: the zonal flow is locked just short of resonance in a stable, stationary configuration.

We do not envisage the equilibrium states we have calculated as entirely stable. Indeed, they cannot be if there is to be transition from one state to another. We hypothesize that in reality the states are metastable—actually baroclinically unstable to smaller scale perturbations—and that the instabilities act to produce an additional forcing which ultimately drives the flow system from the vicinity of an attractor basin of one equilibrium state into that of another. How this occurs cannot be answered with the simple barotropic model we have employed, and we have therefore undertaken similar studies of simple baroclinic flows.

We have refrained from commenting on the geometrical sizes of the flow systems under consideration since we do not necessarily regard the equilibria as global in extent. The existence of large-amplitude meanders of the zonal flow in some regions simultaneously with small-amplitude meanders, or none at all, in others, i.e., high-index and low-index flows existing side by side, suggests that regional stable or metastable equilibria can exist. Such flows would be stable or nearly so to variations of the upstream flow, although the weak coupling through the zonal flows associated with other regional circulations could very well be one of the factors that eventually destroy a quasi-equilibrium circulation. Our studies also suggest that the large-scale forced disturbances may themselves be unstable, leading to regular or irregular fluctuations.

The highly truncated spectral methods are of course only heuristic. One must eventually deal with more accurate models. When there are a fairly large number of degrees of freedom, it is no longer possible to solve the spectral equilibrium equations by algebraic elimination. In this case other methods must be found. One that is global, independent of stability and certain to locate at least one equilibrium point is that of Scarf (1967). Often the method will locate others as well. The conditions for its application can be shown to apply in the present instance. Another method is the false time differencing

scheme of Kalnay-Rivas (1977). Unfortunately, neither method, as stated by their authors, leads to a certain determination of all of the fixed points. The methods must be extended or new ones must be found.

One may also attempt to determine the multiple-equilibria empirically. We have begun such an attempt by looking for the density distribution of the low-frequency flow components in the space of a suitable set of empirical orthogonal functions. The search is being conducted both globally and regionally. Preliminary findings support the idea of multiple equilibria but suggest that the attractor sets may be more complicated than isolated phase points. The regional studies are also in keeping with our view that the stability of a regional configuration isolates it somewhat from flows in other regions. Although the existence of a mean upper circumpolar vortex establishes a coupling between the various regional circulations, the coupling need not always be strong, especially in the tropics and subtropics.

We regard our preliminary findings as useful primarily for their heuristic character, not for their detailed explanations of specific phenomena. They suggest that a stochastic, dynamical system approach, in which the location of equilibrium points, attractor sets, stable and unstable limit cycles, etc., and the study of the stochastic forcing of the system by various instabilities, will become a useful tool for investigation of large-scale atmospheric phenomena. We believe that this approach can lead to a better understanding of large-scale variability, predictability, and climate. To know that a system is in the attractor basin of a stable or metastable equilibrium is to know that it will remain for a time. To know that the system is in a state of transition is to know that it will change more rapidly and be less predictable. Climate itself becomes a question of distributions among possible equilibrium states, and climate variation a matter of how boundary changes lead to altered distributions.

Acknowledgments. The authors wish to express their thanks to Professor Akio Arakawa for his assistance in designing the quasi-geostrophic grid point model used in this study and for several helpful discussions. They also wish to thank Mr. Douglas Sinton for his assistance in adapting and using a shallow water model in preliminary numerical experiments.

REFERENCES

Arakawa, A., 1966: Computational design for long-term numerical integration of the equations of fluid motion: two-dimensional incompressible flow. Part I. *J. Comput. Physics*, **1**, 119–143.

Baur, F., 1951: Extended range weather forecasting. *Compendium of Meteorology*, Amer. Meteor. Soc., 814–833.

Charney, J. G., 1969: A further note on large-scale motions in the tropics. *J. Atmos. Sci.*, **26**, 182–185.

——, 1974: Planetary fluid dynamics. *Dynamic Meteorology*, P. Morel, Editor, D. Reidel, 99–351.

——, and P. G. Drazin, 1961: Propagation of planetary-scale disturbances from the lower into the upper atmosphere. *J. Geophys. Res.*, **66**, 83–109.

Coaker, S. A., 1977: The stability of a rossby wave. *Geophys. Astrophys. Fluid Dyn.*, **9**, 1–17.

Diky, L. A., and G. S. Golitsyn, 1968: Calculation of the Rossby wave velocities in the earth's atmosphere. *Tellus*, **20**, 314–317.

Egger, J., 1978: Dynamics of blocking highs. *J. Atmos. Sci.*, **35**, 1788–1801.

Elliott, R. D., 1951: Extended range forecasting by weather types. *Compendium of Meteorology*, Amer. Meteor. Soc., 834–840.

Gill, A. E., 1974: The stability of planetary waves on an infinite beta-plane. *Geophys. Fluid Dyn.*, **6**, 29–47.

Hirota, I., 1971: Excitation of planetary Rossby waves in the winter stratosphere by periodic forcing. *J. Meteor. Soc. Japan*, **49**, 439–448.

Hoskins, B. J., 1973: Stability of Rossby-Haurwitz waves. *Quart. J. Roy. Meteor. Soc.*, **99**, 723–745.

Kalnáy-Rivas, E., 1977: A numerical scheme to solve unstable boundary value problems. *Advances in Computational Methods for Partial Differential Equations*, II, R. Vichnevetsky, Ed., Int. Assoc. for Math. Comput. in Simulation (IMACS), Rutgers University, 264–268.

Lorenz, E. N., 1963: The mechanics of vacillation. *J. Atmos. Sci.*, **20**, 448–464.

——, 1972: Barotropic instability of Rossby wave motion, *J. Atmos. Sci.*, **29**, 258–264.

Namias, J., 1947: *Extended Forecasting by Mean Circulation Methods*. Washington, U.S. Weather Bureau, 89 pp.

——, 1953: *Thirty Day Forecasting: A Review of a Ten-Year Experiment. Meteor. Monogr.*, No. 6, Amer. Meteor. Soc., 83 pp.

Scarf, H., 1967: The approximation of fixed points of a continuous mapping. *SIAM J. Appl. Math.*, **50**, 1328–1343.